A Fast and Accurate Coarse Method for Multipactor Threshold Prediction of RF Filters Under Modulated Signal Excitation

Carlos Alcaide Guillén, Miguel Rodríguez Jódar, Raúl Cervera Marín, Jose V. Morro, *Member, IEEE*, Pablo Soto, *Member, IEEE*, Òscar Monerris, Javier Ossorio, Rafael Mata, Davide Smacchia, Vicente E. Boria, *Fellow, IEEE*, and César Miquel España

***Abstract*— Multipactor is a key high-power effect limiting the system performance for onboard satellite hardware. Although modern particle simulators admit arbitrary geometries and signals as inputs, their practical use is often limited to continuous-wave (CW) excitations. Unfortunately, the multipactor analysis for input-modulated signals normally leads to prohibitively large CPU times, as signal lengths are very large compared to the electron population's evolution time. The Coarse Method is an elegant way of overcoming this limitation, providing a good estimate of the multipactor threshold in reduced CPU times. However, if the input signal is not preprocessed before being analyzed, the method is unable to account for the frequency dependence as it operates with electron dynamics information extracted at a single frequency, leading to biased predictions for narrowband samples as filters. This article proposes an extension to the original Coarse Method implementation by considering the sample response and the modulated signal spectral distribution to account for the frequency dependence. The resulting method is suitable for estimating the multipactor threshold of narrowband samples excited by modulated signals, while keeping the benefits in terms of simplicity, efficiency, and generality of the Coarse Method. The proposed approach is benchmarked against laboratory measurement results, as well as particle simulators and legacy Coarse Method predictions, revealing the advantages of the novel technique and its range of applications.**

***Index Terms*— Microwave filters, modulation, multipactor, particle physics simulation, satellite communications.**

Received 4 March 2025; revised 4 April 2025; accepted 7 April 2025. Date of publication 22 April 2025; date of current version 28 May 2025. This work was supported in part by the Ministerio de Ciencia e Innovación, Unión Europea (UE), under Research and Development Grant TED2021-129196B-C41/AEI/10.13039/501100011033/Unión Europea NextGenerationEU/PRTR and Grant PID2022-136590OB-C41/AEI/10.13039/501100011033/FEDER; and in part by the European Space Agency (ESA) through several research and development activities, including the Project H2020-ESA-007 under Contract 4000126048/18/NL/AS. The review of this article was arranged by Editor M. Blank. *(Corresponding author: Carlos Alcaide Guillén.)*

Carlos Alcaide Guillén, Jose V. Morro, Pablo Soto, and Vicente E. Boria are with iTEAM, Universitat Politècnica de València, 46022 Valencia, Spain (e-mail: calcaide@iteam.upv.es; jomorros@dcom.upv.es; pabsopac@dcom.upv.es; vboria@dcom.upv.es).

Miguel Rodríguez Jódar, Raúl Cervera Marín, Òscar Monerris, Javier Ossorio, Rafael Mata, and Davide Smacchia are with the ESA-VSC European High Power RF Space and Space Materials Laboratories, 46022 Valencia, Spain (e-mail: miguel.rodriguez@val-space.com; raul.cervera@val-space.com; oscar.monerris@val-space.com; javier.ossorio@val-space.com; rafael.mata@val-space.com; davide.smacchia@val-space.com).

César Miquel España is with the European Space Research and Technology Centre of the European Space Agency (ESTEC-ESA), 2200 AG Noordwijk, The Netherlands (e-mail: cesar.miquel.espana@esa.int).

Digital Object Identifier 10.1109/TED.2025.3559910

I. Introduction

THE multipactor effect occurs when free electrons inside an radio frequency (RF) component operating under vacuum conditions, collide successively against the component walls driven by the RF fields [1]. If the electrons impact against the component walls with kinetic energy in the appropriate range to release enough secondary electrons, the electron population increases, eventually causing a discharge. The number of released electrons, called total electron emission yield (TEEY) [2] (when considering both elastic and inelastic collisions), depends on the electron's impact energy [3], [4], [5]. As multipactor is an effect induced by the TEEY, a minimum power level at the input of the component is required to ignite a multipactor discharge [1], [6]. This power level is referred to as the multipactor power threshold, a key parameter limiting the power handling capability of satellite hardware [7].

The increase in the transmitted power levels and the miniaturization of the components (due to the use of higher frequency bands), driven by the ever-increasing capacity demands for satellite communication systems, foster the occurrence of unwanted high-power effects [8]. As multipactor can lead to a wide range of harmful effects [7], estimating the multipactor threshold is key in assessing the suitability of RF devices for space operation. Thus, it is appealing to develop tools that can analyze the power handling capabilities in the design stage, preventing a failure in space qualification tests [9] or during operation.

Multipactor prediction tools have evolved from methods relying on experimental data [10], [11], to complex simulators in which arbitrary geometries and waveform excitations are analyzed. The legacy methods can be improved by accounting for fringing-field effects pushing electrons away from the critical gap [12], [13], [14], considering the nonuniform fields [15] or the statistical nature of the released electrons [16], [17], [18]. In addition, the nonstationary [19] and quasi-stationary theories [20] were introduced to allow predictions for arbitrary nonstationary signal excitations. This allows for reducing the design margins that have traditionally led to over-demanding specifications, thus enabling a cost reduction of the equipment.

SPARK3D [21] and CST Particle Studio (CST-PS) [22] are multipactor analysis simulators [13], [23], [24], [25], [26] which can cope with arbitrary waveform signals. However, the analysis of RF samples under modulated signal excitation leads to prohibitively long particle simulations [7], as the duration of the signals is much larger than the time required for igniting a multipactor discharge. To speed up the simulations, the Coarse Method was introduced [27], [28], [29]. This method, however, neglects the frequency dependence of the samples, as it only uses information extracted at a single frequency. This is problematic for RF filters, which present a marked dependence on the frequency. The same situation arises in commercial particle simulators using steady-state electromagnetic (EM) fields, such as SPARK3D, which only considers the EM fields at the carrier frequency for modulated signal excitation. Those simulators that compute time-domain EM fields, such as CST-PS, require however very fine simulation time steps, since as the minimum mesh size decreases (to correctly model the minimum geometric details required for obtaining accurate results), the time step must be reduced accordingly in order to comply with the Courant–Friedrich–Lewy (CFL) criterion [30], thus leading to outstandingly resource-demanding simulations even for short signal sections [7]. Nowadays, there is no method available to obtain reliable multipactor threshold predictions in RF filters excited by modulated signals.

A potential approach would consist of obtaining the signal envelope at the critical gap (affected by the frequency dependence of the sample) before the application of the Coarse Method. A direct computation of the critical gap voltage, using time-domain (due to the CFL criterion) or frequency-domain (due to the large number of points required for the inverse Fourier transform) simulators is unpractical for RF filters, as a large computational effort is required. Equivalent circuits can be used instead, but this poses limitations in terms of generality and accuracy. First, the derivation of a suitable equivalent circuit is strongly structure-dependent and involves important simplifications. This explains the wide range of equivalent circuits available in the technical literature to try to model in a simple way the main characteristics of each particular device. Second, once the voltage at the proper location inside the equivalent circuit has been obtained, it must be translated into the critical gap voltage in the EM structure, and must also be related to the power at the input port of the real device. As a result, a specific path must be laid out for each particular structure, which also implies significant approximations.

As a practical alternative, this work proposes an engineering tool based on the Coarse Method to account for the fact that band-limited devices are frequency dependent [31] in an agnostic fashion, as the presented algorithm does not have to resort to particular circuital models or additional cumbersome EM simulations to account for the frequency dependence. As a result, the simplicity, efficiency, and generality of the original Coarse Method can be preserved.

II. Theory

This section provides a complete overview of the legacy version of the Coarse Method [27]. Next, the theory for the extended Coarse Method implementation able to consider the frequency dependence of RF filter samples is detailed in Section II-B.

A. Coarse Method

As to describe the mathematical foundations of the Coarse Method, it is convenient to define the equivalent baseband form of the passband modulated signal at the input of the component

$$x_{\mathrm{bb}}(t) = I(t) + jQ(t) = A(t)e^{j\Phi(t)} \tag{1}$$

where $I(t)$ and $Q(t)$ are the signal in-phase and quadrature (IQ) components. $A(t)$ and $\Phi(t)$ are the envelope and phase of the signal, respectively, given by

$$A(t) = \sqrt{I^2(t) + Q^2(t)};\ \ \Phi(t) = \mathrm{ang}(I(t) + jQ(t)) \tag{2}$$

so that the modulated input signal can, therefore, be expressed as

$$x_{\mathrm{mod}}(t) = \Re\mathfrak{e}\left\{x_{\mathrm{bb}}(t)e^{j2\pi f_{\mathrm{c}}t}\right\} = A(t)\cos(2\pi f_{\mathrm{c}}t + \Phi(t)) \tag{3}$$

where f_c is the reference frequency used for the baseband conversion.

The channel bandwidth in satellite applications is much lower than the carrier frequency. In fact, the relative bandwidth of narrowband devices, such as filters, are rarely larger than 6%–7%. This implies that the signal envelope has much slower variations than the RF carrier, allowing to define an envelope "instantaneous" power in the form

$$P_x(t) = P_0A^2(t) \tag{4}$$

where P_0 is the scaling factor enabling to represent different mean powers, as the baseband signal is normalized in this work so that the maximum of its envelope $A(t)$ is set to one.

A second key concept is that for an RF structure under continuous-wave (CW) excitation, the electron population evolution with time is known to increase or decrease exponentially [27], [29], namely,

$$N(t) = N_0 \exp(\alpha t) \tag{5}$$

where $N(t)$ is the electron population at time instant t, N_0 is the initial electron population, and α (Hz) is the so-called growth factor taking real positive or negative values (representing a population growth or decrease, respectively).

For each power level at the input port, a growth factor α can be fit to the electron population evolution with time. This is accomplished by applying the natural logarithm to the electron population curve obtained from a particle simulation on the structure, considering a CW excitation at the frequency f_{c}.

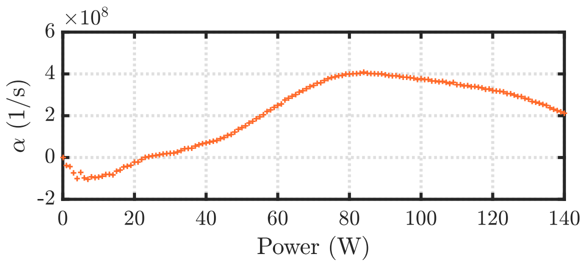

Fig. 1. Growth factor value versus CW excitation power.

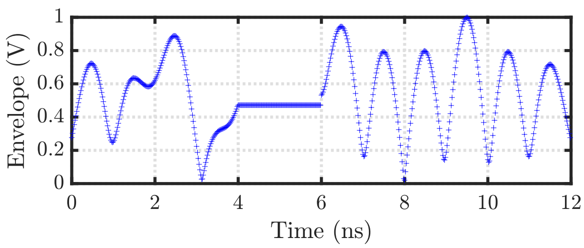

Fig. 2. Samples (with dots) of the signal envelope.

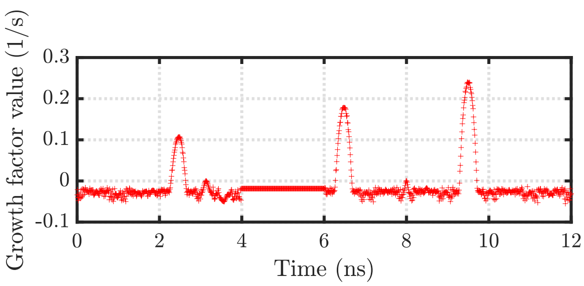

Fig. 3. Growth factor assignment for each signal sample in terms of time, for a certain mean power level of the input signal. Note that the positive growth factors correspond to the regions around the higher peaks of the signal envelope.

This allows for a least mean square fitting of the simulated data to a linearized version of (5), from where the growth factor can be easily derived. The process is repeated for a set of power levels covering the range of interest. Accordingly, a curve like the one shown in Fig. 1 is produced. The CW multipactor threshold corresponds to the lowest power level where the growth factor becomes positive.

From the envelope $A(t)$ and the power scaling factor P_0, an "instantaneous" power (integrating the oscillations of the RF carrier) can be defined in terms of time (see (4)). Then, a growth factor can be assigned to each time instant, in terms of the corresponding "instantaneous" power level, representing the exponential variation of the electron population for this time instant. This process is illustrated graphically in Fig. 2, plotting the samples of the signal envelope, and in Fig. 3, showing the growth factor assigned for each sample. Note how the maximum growth factor values around 2.5, 6.5, and 9.5 ns in Fig. 3 correspond to the maximum envelope values in Fig. 2.

Having access to the array of growth factors represented in Fig. 3, it is possible to search for the maximum sum subarray within the array [29]. Let us suppose that this maximum sum subarray spans from mT_s to a time instant nT_s, being T_s the sampling period. Then, the maximum increase ratio in the electron population is

$$\frac{N(nT_s)}{N(mT_s)} = \exp\left(\sum_{i=m}^{n} \alpha_i T_s\right) = \exp\left(T_s \sum_{i=m}^{n} \alpha_i\right) \tag{6}$$

so that for an electron population increase ratio above some predefined threshold (for instance, a 1000-fold increase is used throughout this work and in [7]), a multipactor discharge is considered to occur.

The step-by-step algorithm implementing the legacy Coarse Method employed in this work is described in the following steps.

1) Obtain the growth factors for CW excitation at the selected reference frequency, hence characterizing how the growth factor changes with the input power (see Fig. 1).
2) Find the CW multipactor threshold for the structure under analysis $P_{\text{th,CW}}$ (i.e., the input power level where the growth factors turn positive).
3) The scaling factor P_0 in (4) is set to $P_{\text{th,CW}}$. In this case, only the sample representing the maximum value of the signal envelope provides a positive growth factor (the remaining ones being negative). This power level is thus a lower bound for the multipactor threshold P_{th} associated with the excitation signal.
4) The complete signal sequence is scaled with a predefined factor, and a search to determine if any subsequence within the signal fulfills the multipactor condition at such a power level is performed. If so, the search is ended. Otherwise, the scaling factor is updated and the search is performed again until the multipactor condition is reached.

B. Extended Coarse Method

The growth factors in the traditional Coarse Method, as detailed in Section II-A, are computed at the same frequency (typically f_c), as the method was initially applied to wideband RF samples [27], for which the frequency response is nearly invariant.

When analyzing RF narrowband samples with frequency-dependent responses, it is appealing to combine information from different frequencies. This is indeed the case of RF filters, the object of this work, which store more energy at the band-edges than at the center of the passband [7], [31], [32].

Since the shape of any passband RF filter response has three clearly identifiable zones, the central region (where the group delay is almost flat) and the band-edges, as shown in Fig. 4, the proposed procedure consists in computing the growth factors at three representative frequencies and combining them according to (7). The goal is to derive an effective growth factor that represents, for its corresponding input power level, the overall behavior considering the frequency dependence of the structure and the spectral distribution of the signal. Note also that for computing each set of growth factors, the EM fields at the critical gap for its corresponding frequency are considered, and linked to the power at the device input, so that the effect of the transfer function between the input and the critical gap at such a frequency is indeed included in the proposed method. Therefore, the frequency dependence effect of the filter is

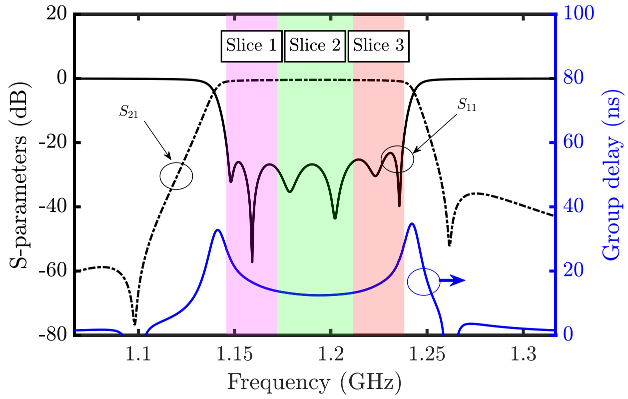

Fig. 4. S-parameters magnitude (dB) and group delay (ns) with a possible spectral slicing scheme composed of three slices.

being considered without having to resort to computing the signal in the critical gap using time-domain EM modelers, which struggle to provide convergent S-parameter results and, therefore, fail in providing an accurate representation of such a waveform within a reasonable computational effort. In this context, note that the formula in (7) is based on a weighted sum, to account for how the energy of the signal under analysis is distributed

$$\alpha_{\mathrm{tot}} = \alpha_{\mathrm{lbe}} w_{\mathrm{lbe}} + \alpha_{\mathrm{cf}} w_{\mathrm{cf}} + \alpha_{\mathrm{ube}} w_{\mathrm{ube}}. \tag{7}$$

Thus, it is necessary to define and obtain the following parameters.

1) Frequencies for which the growth factors are obtained f_{lbe}, f_{cf}, and f_{ube} (i.e., lower band edge, central frequency, and upper band edge).
2) Growth factors α_{lbe}, α_{cf}, and α_{ube}.
3) Weighting coefficients w_{lbe}, w_{cf}, and w_{ube}.

Once the frequencies are determined, α_{lbe}, α_{cf}, and α_{ube} are obtained for each frequency. An in-depth explanation of how to obtain the parameters in (7) is provided in the following subsections.

1) Procedure to Obtain the Simulation Frequencies: The frequency choice for the growth factor computation shall reflect the spectral distribution of the stored energy in the sample, as larger energy implies higher EM fields, and therefore a lower multipactor threshold. This involves the sample's S-parameters and the signal's energy distribution. In this regard, the group delay (i.e., the time the energy takes to pass from the input to the output filter port) can be of help in choosing the frequencies at which the growth factors are to be computed, as it is equal to the ratio between how much energy is stored and the available input power at the device input for CW excitation [31].

As multipactor is a voltage-driven effect, the peak voltage in the critical gap for a CW excitation of 1 W of mean input power, $V_{1\mathrm{W}}$, can be combined with the peak voltage level required for a discharge, V_{th}, to derive the multipactor threshold power in the form

$$P_{\mathrm{th}} = 1\ \mathrm{W} \cdot \left(\frac{V_{\mathrm{th}}}{V_{1\mathrm{W}}}\right)^2. \tag{8}$$

The peak threshold voltage V_{th} can be obtained from charts using reported experimental data or from particle simulation tools. Note that V_{th} depends on the material of the surfaces involved in the most multipactor-prone region where the discharge is expected to occur.

$V_{1\mathrm{W}}$ can be obtained by exploiting the time-averaged stored energy (TASE) concept applied to a structure region including the critical gap [7], [33]. The TASE denotes the summation of the mean electric and magnetic stored energies during a CW excitation cycle. The peak voltage $V_{1\mathrm{W}}$ inside the critical gap can be estimated from the peak gap voltage for a TASE of 1 J, $V_{1\mathrm{J}}$, inside a region of the structure including the critical gap, and the TASE for this analysis region with a CW excitation signal of 1 W of mean power, $\mathrm{TASE}_{1\mathrm{W}}$, at the input port of the complete structure

$$V_{1\mathrm{W}} = V_{1\mathrm{J}} \cdot \sqrt{\frac{\mathrm{TASE}_{1\mathrm{W}}}{1\ \mathrm{J}}} \tag{9}$$

so that, using (9) into (8), the power threshold can be expressed as

$$P_{\mathrm{th}} = 1\ \mathrm{W} \cdot \left(\frac{V_{\mathrm{th}}}{V_{1\mathrm{J}}}\right)^2 \frac{1\ \mathrm{J}}{\mathrm{TASE}_{1\mathrm{W}}}. \tag{10}$$

Note how P_{th} is inversely proportional to the TASE of the filter. As the group delay, GD, is proportional to the TASE [31], it follows:

$$P_{\mathrm{th}} \propto \frac{1}{\mathrm{GD}}. \tag{11}$$

From this reasoning, it is possible to select the frequencies at which the growth factors are computed. The idea is to divide the frequency response into three regions (central slice and band edge slices) using the group delay information, as shown in Fig. 4. A set of growth factors α_i is then obtained at a representative frequency for slice i (f_{lbe}, f_{cf}, or f_{ube}), modeling how the electron population evolves in terms of the input power for the corresponding part of the filter response. Finally, the set of growth factors is weighted considering how the signal energy is distributed along the three slices, obtaining an effective growth factor aimed at capturing the overall behavior. From this point on, the same steps of the traditional Coarse Method approach are applied (see Section II-A), with the significant difference that the weighted growth factors are used instead of the ones computed at a single frequency. The step-by-step procedure proposed to obtain the slices and relevant frequencies is as follows.

1) The frequency f_{cf} is set to the center frequency of the passband. Evaluate the group delay $\mathrm{GD}_{\mathrm{cf}}$ at such a frequency.
2) Find the two frequencies within the passband for which the difference between the group delay at the central frequency and the group delay at these frequencies is x dB. This x dB difference in the group delay should translate into an x dB threshold difference following (11).
3) The center slice is then defined as the frequency band for which the difference is under x dB.
4) The slices for the lower and upper band edges span from the central slice boundaries to the edges of the passband.
5) To compute f_{lbe}, an array containing the square magnitude of the signal fast Fourier transform (FFT) values for the slice 1 frequency bins (see Fig. 4) is considered. This array is normalized by the sum of the array elements, hence obtaining the relative energy of each frequency

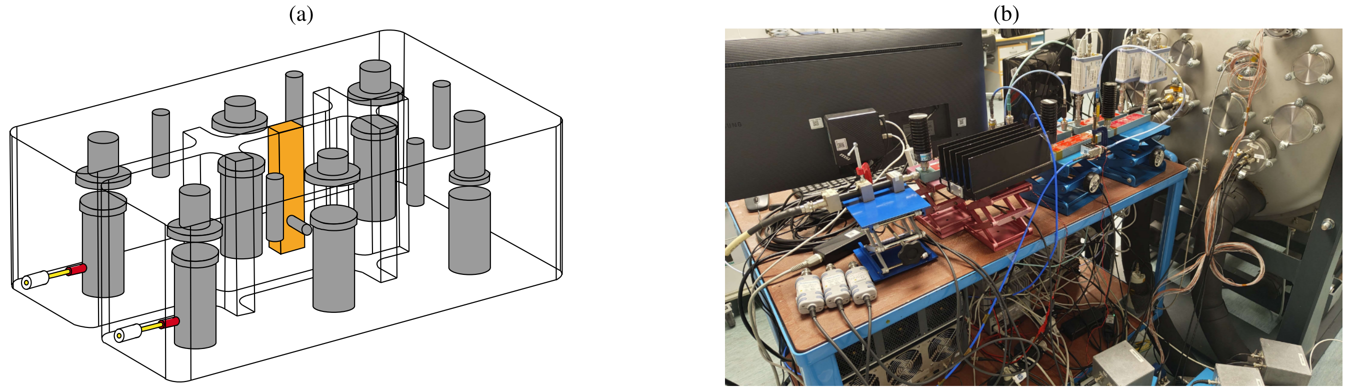

Fig. 5. Illustration of (a) E1 filter and its (b) experimental setup.

bin within slice 1. Next, the resulting array is multiplied by the frequency array for slice 1, thus obtaining a "weighted" frequency array that accounts for the energy content of the signal along the slice. Finally, the sum of this final array provides f_{lbe}. The frequency f_{ube} is computed analogously for slice 3.

The key step in this procedure is the choice of the parameter x, which can be fine-tuned to optimize the results. This value would depend on several factors, such as the peak group delay or the spectral distribution of the signal. A lower limit should be around 0.2 dB (this is the accuracy of the sensors to measure the power threshold in the test bed in [34], as described in [7]). Note also that a large value of x (for instance, 0.5 dB in the examples considered in Section III-B) would result in an overly broad central frequency slice, implying a relevant variation of the EM fields within the slice with respect to the center frequency (where the growth factors are computed).

The use of more spectral slices is not recommended, due to the increase in complexity and computational burden without a relevant benefit in terms of accuracy, as three frequency points properly chosen are enough to capture the main effects of a bandpass filter. For low- or high-pass filters, however, this number could be reduced to two (one in the band edge and another for the rest of the passband) as its group delay response presents only one peak instead of two.

2) Procedure to Obtain the Weighting Coefficients: The coefficients w_{lbe}, w_{cf}, and w_{ube} are assigned in terms of the spectral distribution of the input signal in the following way.

1) Calculate the signal power at each slice: P_{lbe}, P_{cf}, and P_{ube}.
2) Compute the coefficients by normalizing the powers with respect to the overall input power.

As the procedure can effectively obtain the electron population evolution with time along all the signals, it is able to identify both long and short-term multipactor discharges satisfying (6).

III. Methodology and Implementation

The extended Coarse Method has been implemented to estimate the multipactor threshold of a set of RF samples excited with modulated signals. The resulting predictions are then compared with the ones provided by the legacy Coarse Method and by a commercial particle simulator, and also with the measured thresholds.

TABLE I
Characteristics of the Input Signals (Band, PAPR, and Spectral Distribution of the Energy)

Signal	Band	PAPR (dB)	Energy distribution
1	E5	5.8	$\sim$ 80% around f_0
2	E5	4.0	$\sim$ 60% close band-edges
3	E6	6.0	$\sim$ 80% around f_0
4	E6	3.7	$\sim$ 60% close band-edges
5	E1	6.2	$\sim$ 50% around f_0
6	E1	4.2	$\sim$ 60% close band-edges

A. Signals and RF Samples for Results Validation

Three comb-line filters made of bare aluminum are to be used for the tests to prove the correct operation of the proposed prediction approach. The filters employed are six-pole comb-line filters with two symmetrical transmission zeros designed to operate in the E5, E6, and E1 Galileo bands centered at 1191.8, 1278.8, and 1575.5 MHz, respectively. The E6 and E1 band filters have a 50-MHz bandwidth, whereas the E5 band filter has a 92-MHz bandwidth (see Fig. 5(a) for a schematic representation of the E1 filter). The filters have been designed to have the multipactor discharge in the gap between a resonator post and the base of its corresponding tuner.

Each of the three filters is to be excited with two different signals, thus resulting in six case studies. The most relevant characteristics of the signals are compiled in Table I. Note that the six signals are 1 ms long, whereas the carrier period is under 1 ns, so that the discharge at the multipactor threshold is typically sustained within a signal segment significantly shorter than the whole signal duration.

The typical spectrum of the odd-numbered signals, those with the energy concentrated around the passband center (where the group delay is almost flat), is included in Fig. 6(a). Conversely, the appearance of the even signals, with a large amount of energy close to the band edges, is more like the one shown in Fig. 6(b).

B. Implementation

The Coarse Method presented in [29] has been extended following the theory described in Section II-B. The growth factors are computed at the three frequencies provided by the proposed algorithm, and are combined according to the signal energy distribution. To define the three spectral regions, the parameter x has been set to 0.2 dB.

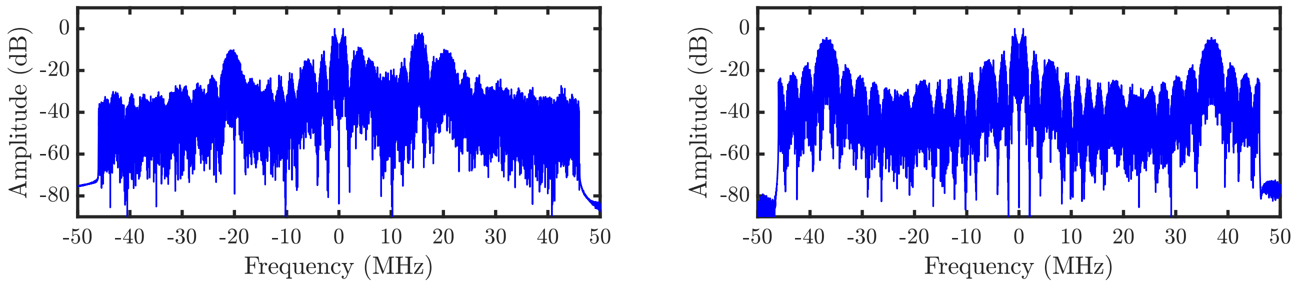

(a) (b)

Fig. 6. Typical spectrum of a signal with a higher energy concentration (a) around the center of the passband and (b) close to the band-edges.

TABLE II

ENHANCED COARSE METHOD GROWTH FACTORS COMPUTATION FREQUENCIES AND CORRESPONDING WEIGHTING COEFFICIENTS

Filter	Enhanced Coarse Method Parameters					
	Frequencies (MHz)			Coefficients		
E5 (signal 1)	1170.3	1191.8	1213.9	0.0816	0.8305	0.0878
E5 (signal 2)	1155.2	1191.8	1228.8	0.3089	0.3819	0.3092
E6 (signal 3)	1260.6	1278.8	1294.4	0.0080	0.7879	0.2041
E6 (signal 4)	1263.0	1278.8	1294.6	0.2896	0.4203	0.2900
E1 (signal 5)	1564.3	1575.5	1590.2	0.0756	0.5098	0.4146
E1 (signal 6)	1555.2	1575.5	1595.8	0.3101	0.3801	0.3098

The growth factors were computed from the electron population evolution with time provided by SPARK3D CW simulations (according to the procedure described in Section II-A). The analysis was bounded to just the critical gap inside the actual sample under analysis, and used the standard general configuration detailed in [7] (the seeding density was above 10^9 electrons/m^3 to ensure convergence). CW particle simulations for mean input powers spanning from 1 to 160 W at the filter input port were run in SPARK3D. For each input power, the electron evolution with time was hence obtained. Finally, the fitting described in Section II-A is applied to obtain a plot similar to the one in Fig. 1.

For this study, both Coarse Methods implementations assume a multipactor discharge occurs when the electron population increases by a factor of 1000. The TEEY of the surfaces limiting the critical gap was measured (with the experimental setup and facilities described in [35]) and used for the simulations. These TEEY measurements were performed a few days before the multipactor tests, to minimize the TEEY aging effect for enhancing the simulation faithfulness.

In the extended Coarse Method implementation, the frequencies at which the growth factors are computed and the coefficients to use in (7) are shown in Table II. Although the same slicing is applied to the two signals exciting the same filter, the frequencies where the growth factors are computed for slices 1 and 3 differ as the spectral distribution of both signals is not the same. Note how for signals 2, 4, and 6, the sum of the first and last coefficients is about 60%, being similar to the amount of power close to the band-edges (see Table I).

C. Experimental Setup

All multipactor tests were carried out using a state-of-the-art multipactor test bed, capable of coping with both CW and modulated signals. The test bed does not include the classic microwave nulling system, conceived for CW operation, as it only performs properly in very narrowband applications. Instead, an IQ detection method has been implemented [34]. The input signal is injected using a Keysight PXI-MP1 M9383A Signal Generator. This signal is fed into the device under test (DUT) and placed inside the vacuum chamber, where three R&S NRQ-6 power sensors are employed to monitor the power at three different points. One is used to measure the input power to the DUT, the second is used to monitor the reflected power, and the third is used to monitor the DUT output power. The electrometer and the IQ detection methods were the more sensitive ones, allowing to identify the multipactor breakdown power threshold. Note also that Strontium electron seeding radioactive sources were employed to improve the statistical reproducibility of the experiment. A picture of the experimental test bed with the DUT placed inside the vacuum chamber is provided in Fig. 5(b). The block diagram of the test bed is essentially the one shown in [34, Fig. 8].

IV. RESULTS DISCUSSION

This section confronts the measured and predicted thresholds, and analyzes the causes of the differences reported. Table III compares the predictions from both Coarse Method algorithms with the measured multipactor thresholds. The standard Coarse Method results are obtained using growth factors computed at the central frequency of each band. The results from the extended Coarse Method are retrieved following the implementation described in Section III-B. In addition, Table III also includes the predicted thresholds from SPARK3D multipactor modulated signal simulations, where the signal modulates the steady-state EM fields at a single frequency externally provided to SPARK3D. For each filter, the steady-state fields at the center and lower passband frequencies were computed with the frequency domain CST solver. A particular EM field was imported in SPARK3D to perform each modulated signal particle simulation. These simulations were initiated at the starting time instant of the critical part of the signal identified by the Coarse Method.

Since the time variation of the signal envelope affects to the evolution of the electron population with time, the time-response of the test-bed sensors plays a role in the detection of multipactor and the measured thresholds. To replicate the effect of the nonzero time response of the detection methods in simulations, the software tool is updated so that the 1000-fold increase in the electron population must be sustained for at least 200 ns to declare a discharge. This condition can

TABLE III
COMPARISON OF THE MEASURED THRESHOLDS WITH THE PREDICTED ONES FOR LEGACY AND THE EXTENDED COARSE METHODS, SPARK3D SIMULATIONS MODULATING THE STEADY-STATE EM FIELDS COMPUTED AT THE CENTER f_0 AND LOWER FREQUENCY f_{c1} OF THE FILTER PASSBAND (DELTAS COMPARED TO THE EXPERIMENTAL THRESHOLDS IN BOLD)

Filter	Measured (W)	Coarse (W)	Extended Coarse (W)	SPARK3D @ f_0 (W)	SPARK3D @ f_{c1} (W)
E5 (Signal 1)	16.90	17.61 **(+0.18 dB)**	17.51 **(+0.15 dB)**	15.75 **(-0.31 dB)**	5.25 **(-5.08 dB)**
E5 (Signal 2)	15.10	19.59 **(+1.23 dB)**	13.90 **(-0.40 dB)**	17.75 **(+0.70 dB)**	5.75 **(-4.19 dB)**
E6 (Signal 3)	14.00	14.99 **(+0.30 dB)**	14.19 **(+0.06 dB)**	14.75 **(+0.23 dB)**	6.25 **(-3.56 dB)**
E6 (Signal 4)	15.10	17.99 **(+0.76 dB)**	15.47 **(+0.11 dB)**	16.25 **(+0.32 dB)**	7.25 **(-3.29 dB)**
E1 (Signal 5)	21.40	25.42 **(+0.75 dB)**	24.87 **(+0.65 dB)**	23.25 **(+0.36 dB)**	7.75 **(-4.41 dB)**
E1 (Signal 6)	19.00	26.09 **(+1.38 dB)**	20.85 **(+0.40 dB)**	24.75 **(+1.15 dB)**	8.75 **(-3.37 dB)**

be applied in both Coarse Method implementations. However, the SPARK3D automatic threshold determination tool does not consider the time lapse for which the electron population is over a predefined threshold. In SPARK3D, simulations in 0.5-W power steps have been used instead, and a visual inspection of the electron population with time trace is performed to check if the criterion is fulfilled. Thus, the uncertainty of SPARK3D predicted thresholds is ±0.25 W.

As Table III reveals, the choice of the EM fields has a very significant impact on the SPARK3D predictions. This is due to the frequency dependence of the TASE [7], [31]. The EM fields at the lower band-edge have higher intensity due to the larger TASE at such a frequency, leading to a lower multipactor threshold in virtue of (10). Note that the value of the growth factors is also affected by the TASE (altering the power axis mainly). Since the modulated signals extend along all the filter passband, the use of the EM fields at the passband frequency with the largest TASE leads to extremely conservative predictions (last column in Table III), with predicted thresholds about 3 to 5 dB lower than the measured ones.

Conversely, the SPARK3D multipactor modulated signal simulations using the EM fields at the passband center frequency f_0 (see the penultimate column in Table III), where the lowest TASE value in the passband is obtained, should provide optimistic predictions. However, they must be very close to the real ones for the odd-numbered signals, whose energy is mainly located in the center of the filter passband (see Table I). This is observed in Table III for signals 3 and 5. Nonetheless, the SPARK3D threshold is slightly below the measured one for signal 1. This effect is attributed to the accuracy of the experimental test-bed (within ±0.6 dB). For the remaining signals (i.e., the even ones), with more energy close to the band edges, the SPARK3D predictions increase compared to the corresponding odd-numbered signal instead of decreasing as in the experimental data. This is because SPARK3D detects the effect of the lower peak-to-average power ratio (PAPR) of the even-numbered signals in Table I (which increases the threshold), but is unable to capture the effect associated with the distribution of the signal spectral content (which pushes down the threshold) as it only considers the EM fields at f_0. The filter E6 case is different, as the band-edge energy is closer to the passband central region, as revealed by the fact that f_{lbe} and f_{ube} in Table II are closer to f_0 in signal 4 than in signals 2 and 6, leading to growth factors more similar to the ones obtained at the central frequency.

The same analysis for SPARK3D simulations applies to the traditional Coarse Method results, as its growth factors are computed only from information extracted at f_0 (note in Table III how the thresholds provided by this technique replicate the SPARK3D ones with a mean increase of about 0.35 dB). This issue is effectively solved by the extended implementation of the Coarse Method thanks to its more elaborated way of obtaining the growth factors (by combining information from f_0 and the band edges), which captures both effects (PAPR and signal spectral distribution) and reproduces the qualitative trend in the measurements in all cases. In fact, this technique is the one providing the predicted thresholds closer to the measured ones in all the scenarios (except for the odd-numbered signal 5, where SPARK3D is slightly more accurate). It must be highlighted how the legacy Coarse Method deviations show a relevant increase for the even-numbered signals (and particularly, for signals 2 and 6) as it neglects the effect of the energy located close to the band-edges which causes a reduction in the threshold.

Regarding the CPU time assessment, the legacy Coarse Method typically takes about 2 h (mainly for simulations for growth factor computation). Since the extended Coarse Method must compute the growth factors at three different frequencies, the computational effort triples. However, the procedure can be parallelized in a single computer, allowing in practice to obtain the predictions in the same amount of time as the traditional Coarse Method implementation by running three SPARK3D instances at the same time. On the other hand, a single SPARK3D modulated signal simulation can take about 24 h on average. More importantly, the seeding time instant of the SPARK3D simulation must be determined beforehand (so that the analysis is limited to only the critical part of the signal), otherwise the computational effort is unaffordable. In contrast, both Coarse Method implementations analyze the whole sequence for all the seeding time instants simultaneously. All the CPU times reported in this work have been obtained in an Intel i9-9900K computer equipped with 8 cores of 3.6-GHz base frequency and with 128 GB of RAM.

V. CONCLUSION

In this article, a technique for extending the capabilities of the Coarse Method for narrowband structures has been presented, and its correct operation has been demonstrated by comparing measured and predicted thresholds. The use of the extended Coarse Method implementation effectively reduces the prediction error, particularly for those signals with relevant spectral content in the band edges, due to the use of information from three frequencies distributed along the passband. The corresponding threefold increase in the CPU time can be compensated by a parallelization of the algorithm.

Since the extended Coarse Method implementation enables, for the first time, fast accurate multipactor threshold predictions for narrowband components excited with arbitrary signals, it is a practical alternative to particle simulators for modulated input signals. It is worth pointing out that the proposed method can process long signal sequences, in a fraction of the time required by a particle simulator to track only a few tens of nanoseconds of the full signal from a predefined seeding time instant. Moreover, it provides more accurate predictions than those particle simulators which only consider information extracted at a single frequency, especially for signals with a significant part of its energy near the filter band edges.

Acknowledgment

The authors would like to acknowledge the ESA-VSC European High Power RF Space Laboratory for its contribution to this work—a laboratory funded by the European Regional Development Fund—a way of making Europe.

References

[1] J. R. M. Vaughan, "Multipactor," *IEEE Trans. Electron Devices*, vol. ED-35, no. 7, pp. 1172–1180, Jul. 1988, doi: 10.1109/16.3387.

[2] N. Fil, M. Belhaj, J. Hillairet, and J. Puech, "Multipactor threshold sensitivity to total electron emission yield in small gap waveguide structure and TEEY models accuracy," *Phys. Plasmas*, vol. 23, no. 12, Dec. 2016, Art. no. 123118, doi: 10.1063/1.4972571.

[3] J. R. M. Vaughan, "Observations of multipactor in magnetrons," *IEEE Trans. Electron Devices*, vol. ED-15, no. 11, pp. 883–889, Nov. 1968, doi: 10.1109/T-ED.1968.16532.

[4] M. Furman and M. Pivi, "Probabilistic model for the simulation of secondary electron emission," *Phys. Rev. Special Topics-Accel. Beams*, vol. 5, no. 12, Dec. 2002, Art. no. 124404, doi: 10.1103/physrevstab.5.124404.

[5] C. Vicente et al., "Multipactor breakdown prediction in rectangular waveguide based components," in *IEEE MTT-S Int. Microw. Symp. Dig.*, Jan. 2005, pp. 1055–1058, doi: 10.1109/MWSYM.2005.1516852.

[6] R. M. Vaughan, "Secondary emission formulas," *IEEE Trans. Electron Devices*, vol. 40, no. 4, p. 830, Apr. 1993, doi: 10.1109/16.202798.

[7] P. González et al., "Multipactor threshold estimation techniques based on circuit models, electromagnetic fields, and particle simulators," *IEEE J. Microw.*, vol. 2, no. 1, pp. 57–77, Jan. 2022, doi: 10.1109/JMW.2021.3132284.

[8] M. Yu, "Power-handling capability for RF filters," *IEEE Microw. Mag.*, vol. 8, no. 5, pp. 88–97, Oct. 2007, doi: 10.1109/MMM.2007.904712.

[9] *Multipaction Design Test*, Standard ECSS-E-ST-20-01C, European Cooperation for Space Standarization, 2020.

[10] A. Woode and J. Petit, "Diagnostic investigations into the multipactor effect, susceptibility zone measurements and parameters affecting a discharge," ESA, Noordwijk, The Netherlands, Tech. Rep. 1556, 1989.

[11] R. Woo, "Final report on RF voltage breakdown in coaxial transmission lines," NASA, Pasadena, CA, USA, Tech. Rep. 32-1500, Oct. 1970.

[12] R. Udiljak, D. Anderson, M. Lisak, J. Puech, and V. E. Semenov, "Multipactor in a waveguide iris," *IEEE Trans. Plasma Sci.*, vol. 35, no. 2, pp. 388–395, Apr. 2007, doi: 10.1109/TPS.2007.892737.

[13] A. A. Al-Mudhafar, J. Puech, and H. L. Hartnagel, "Investigation of multipactor effect in microwave components in the presence of fringing fields," in *Proc. 44th Eur. Microw. Conf.*, Oct. 2014, pp. 406–409, doi: 10.1109/EUMC.2014.6986456.

[14] V. E. Semenov et al., "Enhancement of the multipactor threshold inside nonrectangular iris," *IEEE Trans. Electron Devices*, vol. 65, no. 3, pp. 1164–1171, Mar. 2018, doi: 10.1109/TED.2018.2798538.

[15] R. Udiljak, D. Anderson, M. Lisak, V. E. Semenov, and J. Puech, "Multipactor in a coaxial transmission line. I. Analytical study," *Phys. Plasmas*, vol. 14, no. 3, Mar. 2007, Art. no. 033508, doi: 10.1063/1.2710464.

[16] N. K. Vdovicheva, A. G. Sazontov, and V. E. Semenov, "Statistical theory of two-sided multipactor," *Radiophys. Quantum Electron.*, vol. 47, no. 8, pp. 580–596, Aug. 2004, doi: 10.1023/b:raqe.0000049556.18329.e9.

[17] R. Cervera-Marín et al., "A genetically based algorithm to improve execution speed in multipactor simulations in parallel-plate waveguides," *IEEE Trans. Electron Devices*, vol. 71, no. 4, pp. 2638–2644, Apr. 2024, doi: 10.1109/TED.2024.3362314.

[18] A. Coves, G. Torregrosa-Penalva, C. Vicente, B. Gimeno, and V. E. Boria, "Multipactor discharges in parallel-plate dielectric-loaded waveguides including space-charge effects," *IEEE Trans. Electron Devices*, vol. 55, no. 9, pp. 2505–2511, Sep. 2008, doi: 10.1109/TED.2008.927945.

[19] S. Anza et al., "RF breakdown prediction for microwave passive components in multi-carrier operation," in *Ultra-Wideband, Short Pulse Electromagn.*, 2010, pp. 375–381, doi: 10.1007/978-0-387-77845-744.

[20] S. Anza et al., "Prediction of multipactor breakdown for multicarrier applications: The quasi-stationary method," *IEEE Trans. Microw. Theory Techn.*, vol. 60, no. 7, pp. 2093–2105, Jul. 2012, doi: 10.1109/TMTT.2012.2197021.

[21] SPARK3D. (2024). *Dassault Systemes*. [Online]. Available: https://www.3ds.com/products-services/simulia/products/spark3d

[22] CST. (2024). *Studio Suite. Dassault Systemes*. [Online]. Available: https://www.3ds.com/products-services/simulia/products/cst-studio-suite

[23] S. Anza et al., "Recent developments on FEST3D/SPARK3D simulation tools," in *Proc. Int. Workshop Multipactor, Corona Passive Intermodulation Space RF Hardw. (MULCOPIM)*, Sep. 2014, pp. 1–5.

[24] F. Teberio et al., "Waveguide band-pass filter with reduced sensitivity to fabrication tolerances for Q-band payloads," in *IEEE MTT-S Int. Microw. Symp. Dig.*, Jun. 2017, pp. 1464–1467, doi: 10.1109/MWSYM.2017.8058897.

[25] J. Vague et al., "Multipactor effect characterization of dielectric materials for space applications," *IEEE Trans. Microw. Theory Techn.*, vol. 66, no. 8, pp. 3644–3655, Aug. 2018, doi: 10.1109/TMTT.2018.2845869.

[26] F. Teberio, P. Martin-Iglesias, I. Arregui, I. Arnedo, T. Lopetegi, and M. A. G. Laso, "Compact harmonic rejection filter for C-band high-power satellite applications," in *IEEE MTT-S Int. Microw. Symp. Dig.*, Los Angeles, CA, USA, Aug. 2020, pp. 591–594, doi: 10.1109/IMS30576.2020.9224052.

[27] D. González-Iglesias, Ó. Monerris, B. G. Martínez, M. E. Díaz, V. E. Boria, and P. M. Iglesias, "Multipactor RF breakdown in coaxial transmission lines with digitally modulated signals," *IEEE Trans. Electron Devices*, vol. 63, no. 10, pp. 4096–4103, Oct. 2016, doi: 10.1109/TED.2016.2596801.

[28] O. Koch, "Comparison of multipactor analysis methods for Galileo signals," in *Proc. IEEE Conf. Antenna Meas. Appl. (CAMA)*, Sep. 2018, pp. 1–4, doi: 10.1109/CAMA.2018.8530632.

[29] C. Alcaide-Guillén et al., "Multipactor analysis by exploiting Kadane's method," in *Microw. Medit. Symp.*, pp. 1–6, May 2022, pp. 1–6, doi: 10.1109/MMS55062.2022.9825547.

[30] R. Courant, K. Friedrichs, and H. Lewy, "On the partial difference equations of mathematical physics," *IBM J. Res. Develop.*, vol. 11, no. 2, pp. 215–234, Mar. 1967, doi: 10.1147/rd.112.0215.

[31] C. Ernst, V. Postoyalko, and N. G. Khan, "Relationship between group delay and stored energy in microwave filters," *IEEE Trans. Microw. Theory Techn.*, vol. 49, no. 1, pp. 192–196, Jan. 2001, doi: 10.1109/22.900007.

[32] P. González et al., "A new reference sample for high-frequency multipactor testing," *IEEE Microw. Wireless Technol. Lett.*, vol. 33, no. 6, pp. 675–678, Jun. 2023, doi: 10.1109/LMWT.2023.3239419.

[33] F. M. Vanin, F. De Paolis, and D. Schmitt, "Resonator voltage prediction in microwave bandpass filters," *IEEE Trans. Microw. Theory Techn.*, vol. 63, no. 2, pp. 397–402, Feb. 2015, doi: 10.1109/TMTT.2014.2380311.

[34] O. Monerris-Belda et al., "High power RF discharge detection technique based on the in-phase and quadrature signals," *IEEE Trans. Microw. Theory Techn.*, vol. 69, no. 12, pp. 5429–5438, Dec. 2021, doi: 10.1109/TMTT.2021.3120657.

[35] R. Mata, A. Cros, B. Gimeno, and D. Raboso, "Secondary electron emission yield in thick dielectric materials: A comparison between Kelvin probe and capacitive methods," *J. Phys. D, Appl. Phys.*, vol. 57, no. 40, Jul. 2024, Art. no. 405302, doi: 10.1088/1361-6463/ad5c6f.